Clays and Clay Minerals, Vol. 63, No. 5, 368–377, 2015.

NATIVE MORPHOLOGY OF HYDRATED SPHEROIDAL HALLOYSITE OBSERVED BY ENVIRONMENTAL TRANSMISSION ELECTRON MICROSCOPY

JEREMIE BERTHONNEAU[1,2]*, OLIVIER GRAUBY[1], CHARLOTTE JEANNIN[1], DAMIEN CHAUDANSON[1], EMMANUEL JOUSSEIN[3] AND ALAIN BARONNET[1]

[1] Aix Marseille Université, CNRS, CINaM UMR 7325, 13288 Marseille, France
[2] <MSE>, the CNRS-MIT Joint Laboratory, Massachusetts Institute of Technology, 77 Massachusetts Avenue, Cambridge, MA 02139, USA
[3] Université de Limoges, FST, GRESE, 123 avenue Albert Thomas, 87060 Limoges, France

Abstract—Natural mineral materials such as tabular and spheroidal halloysites have recently been suggested as candidates for intercalating metal ions or organic molecules. Their potential use as nano-adsorbents is related to their porous structure and water content. Although the two morphologies can co-exist in natural deposits, spheroidal halloysites remain poorly characterized whereas much literature exists on tubular halloysites. The present study investigates the native morphology, internal porous structure, and behavior upon dehydration of spheroidal halloysite from Opotiki (New Zealand). This mineral was characterized in its natural hydrated state using a transmission electron microscope equipped with an environmental cell (EC-TEM). The sample was placed in a sealed block in which water vapor-saturated air circulated at a pressure of 30 Torr. The observed particles consisted of almost complete spheroids displaying polyhedral external surfaces. 1:1 layers stack concentrically as a pore-free, onion-like structure. The dynamic processes of dehydration created by slow depressurization of the cell resulted in a decrease in the layer-to-layer distance (d_{001}) from ~10 Å to ~7 Å due to the loss of interlayer water molecules. Irreversible formation of spurious 'internal pores' was recorded during this process. These pores were not indigenous to the hydrated 10 Å halloysite and resulted from the collapse of the native layers. They cannot account for the physical chemical properties of spheroidal halloysite. Spheroidal halloysites would have a lower propensity for intercalating ions or molecules than tubular halloysites. Isolated facets were also observed in high-resolution-TEM and displayed a pseudo-hexagonal morphology. The three-dimensional microstructure of the spheroid appeared bent along the three pseudo equivalent y_i directions of the kaolinite-like single layers. An analogy with polyhedral serpentine has allowed the proposal of a formation process of hydrated spheroidal halloysite triggered by enrichment in divalent ions in the growth system.

Key Words—Crystal Growth, Dehydration Behavior, Nano-adsorbent, Native Halloysite, Transmission Electron Microscopy.

INTRODUCTION

Halloysite is a 1:1 dioctahedral phyllosilicate belonging to the kaolin group. Compared to other minerals from this group (*i.e.* kaolinite, dickite, and nacrite), the naturally occurring form of halloysite contains a notable number of water molecules in the interlayer space. The structural formula can be written as $Al_2(OH)_4Si_2O_5{\cdot}2H_2O$, and the layer-to-layer distance (d_{001}) is ~10 Å. The hydrated form is known as 10 Å halloysite (or endellite) whereas the term 7 Å halloysite (metahalloysite) is used for the often-described dehydrated form (MacEwan, 1948; Churchman and Carr, 1975; Guggenheim, 1977). The 10 Å halloysite undergoes irreversible dehydration at 40ºC under a relative humidity (RH) of 40% and at 65ºC under 100% RH, inducing contraction of d_{001} to 7.2 Å (Alexander *et al.*, 1943; Kohyama *et al.*, 1978). As a consequence, most of the characterization techniques that involve heating or vacuum cause dehydration and do not allow optimal conditions suitable to the study of this mineral in its hydrated state. The water content of 10 Å halloysite is 12.3 wt.%, but the exact position of the water molecules inside the interlayer space has not yet been ascertained (Kohyama *et al.*, 1978).

The presence of water in halloysite is reported to play a significant role in its physical and chemical properties (cation exchange capacity, cation selectivity, and reactivity with organic molecules; see Joussein *et al.*, 2005). Natural mineral materials such as halloysite are considered for environmental and pharmaceutical applications due to their great propensity to intercalate metal ions or organic molecules (Theng, 1974; Joussein *et al.*, 2007; Tan *et al.*, 2014; Kiani, 2014). The morphology and internal porous structure of this mineral are believed to influence directly its potential use as a nano-adsorbent. Hence, a complete characterization of this mineral in its native hydrated state and an understanding of the impact of its hydration-dehydration behavior are of prime importance to test this link.

Diverse morphologies of halloysite are encountered in natural deposits (*i.e.* tubular, spheroidal, and tabular).

* E-mail address of corresponding author:
berthonneau@cinam.univ-mrs.fr
DOI:10.1346/CCMN.2015.0630503

Following the lattice parameter, *b*, the lateral dimensions of the ideal isolated dioctahedral and tetrahedral sheets are 8.62 Å and 8.93 Å, respectively (Bates *et al.*, 1950). When these two sheets are joined, the mismatch can be minimized by (1) layer wrapping (octahedral sheet inward and tetrahedral sheet outward), and/or (2) sheet distortion with rotation and tilt of the tetrahedra. The most common morphologies are tubular and spheroidal, which display layer wrapping (Bates *et al.*, 1950). In the case of tabular halloysite, the mismatch is minimized by the rotation of the tetrahedra (Radoslovich, 1963; Bailey, 1990). Tubular halloysites allow an accommodation of the mismatch only perpendicularly to the tube axis, whereas it is expected to occur in all the directions for spheroidal halloysites. Up to now, no experimental evidence has existed to support this assertion. The crystallographic control on the external morphology of spheroidal halloysite has thus been studied here to understand the differences between the two morphologies.

Halloysite is not the only phyllosilicate in which the mismatch is minimized by layer wrapping. Serpentines (1:1 trioctahedral phyllosilicates) also display tubular (chrysotile) and spheroidal (polyhedral serpentine) varieties (Zega *et al.*, 2006; Baronnet *et al.*, 2007; Andreani *et al.*, 2008). The winding axis differs, however, between tubular halloysite and chrysotile. Chrysotile layers wrap around the crystallographic *x* axis, whereas tubular halloysite layers wrap around the crystallographic *y* axis (Bates *et al.*, 1950; Chisholm, 1992). This difference is related to the octahedral occupancy, which is dioctahedral for kaolin and trioctahedral for serpentine. A complete structural analogy between halloysite and serpentine would help, therefore, to understand the formation of the different morphologies of 1:1 phyllosilicates.

Halloysite forms in several ways; by hydrothermal alteration, and by meteoric weathering, such that it is a major component of newly formed soils from igneous (*i.e.* granite, rhyolite, dolerite, volcanic glass, or pumices) and metamorphic (*i.e.* gneiss, schist, or amphibolite) materials (Sand, 1956; Parham, 1970; Churchman, 2000). The progressive dissolution of feldspar and micas is followed by crystallization of tubular halloysite (Giese, 1991). Spheroidal halloysite comes from the weathering of volcanic ashes (Tomura *et al.*, 1985). A dissolution-crystallization sequence consisting of volcanic ash–allophane–10 Å halloysite– 7 Å halloysite–kaolinite was proposed by Churchman (2000). The ease with which this mineral dehydrates in the soil profile causes its segregation in the deposits. Accordingly, 10 Å halloysites are frequently encountered at depth whereas 7 Å halloysites are encountered closer to the surface.

In the present study, an environmental cell (EC) fitted to a transmission electron microscope (TEM) was used to investigate the native morphology of spheroidal halloysite in its natural state. Hydrated spheroidal halloysite from Opotiki were exposed to water vapor-saturated air inside the TEM chamber. This technique allowed successful observations of polygonized spheroids as well as dynamic observations of the morphological and structural changes during depressurization of the chamber. New insights into the formation of internal pores by dehydration allowed elucidation of their capacity as nano-adsorbents. A complementary investigation of isolated facets of spheroids in conventional HRTEM confirmed their pseudo-hexagonal morphology and also allowed elucidation of the crystallographic condition of wrapping. These findings have enabled a better understanding of the formation process of 1:1 phyllosilicates.

MATERIALS AND METHODS

Origin of the sample

The halloysite studied here was initially described and interpreted as the weathering product of rhyolite deposits near the town of Opotiki (northeast New Zealand) by Kirkman (1977). This type of sample is considered exceptional with respect to its purity and its complete hydration (87% spheroidal particles). Numerous studies have examined this sample (*e.g.* Kohyama *et al.*, 1982; Churchman and Theng, 1984; Delvaux *et al.*, 1990; Churchman *et al.*, 1995; Joussein *et al.*, 2005, 2006). Except for Kohyama *et al.* (1982) and more recently Joussein *et al*. (2006) on dehydration behavior, all these studies were conducted on the dehydrated form due to the methodological problems described above. The formula-unit of this sample in its dehydrated form is $Al_{1.86}Fe_{0.14}(OH)_4Si_{1.98}Al_{0.02}O_5$ (Churchman and Theng, 1984). The sample used in the present study was stored permanently under water in order to prevent dehydration.

Preparation of samples for the environmental cell (EC)

A 0.05 µL drop of the spheroidal halloysite suspension was deposited on a copper grid (d = 3.05 mm, Electron Microscopy Sciences, Hatfield, Pennsylvania, USA) covered by a thin carbon film (Figure 1). A spacer, a second carbon film, and another copper grid were placed on top. The sample was sandwiched between the two carbon films, which ensured isolation from vacuum. The copper grids were pierced with seven holes 0.15 mm in diameter. The transmission of the electron beam was thus allowed only when the holes in the two grids matched. This assembly was adapted to a TEM sample holder (JEOL Ltd™, Tokyo, Japan, Figure 1).

Characterization techniques

The EC-TEM observations were conducted using a JEM 3010 TEM (JEOL Ltd™, Tokyo, Japan), fitted with a LaB_6 electron gun, and under a 300 kV accelerating voltage. The experimental setting consisted of a classical TEM into which the gas-tight cell was inserted. This cell

https://doi.org/10.1346/CCMN.2015.0630503 Published online by Cambridge University Press

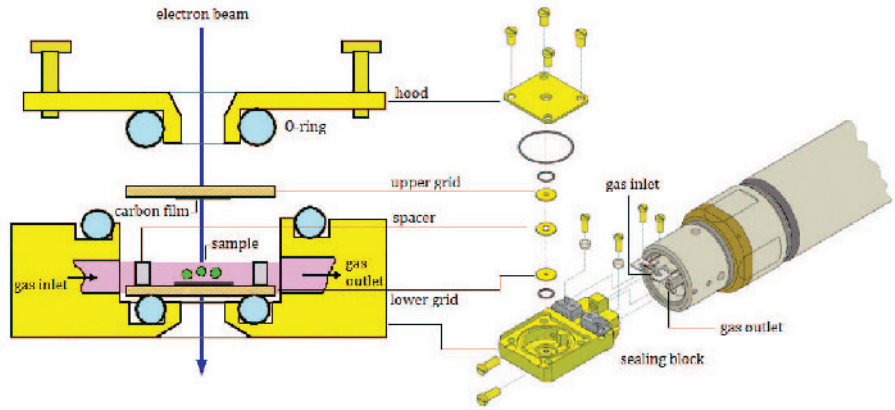

Figure 1. Disjoint sketch of the environmental cell (EC) used as sample holder (provided by JEOL Ltd™, Tokyo, Japan).

held the sample and allowed the circulation of a gas flux controlled by an environmental system (Figure 1). A maximum total gas pressure of 6.7 kPa (50 Torr) can be maintained within the flat chamber, the thickness of which corresponds to the spacer thickness (0.1 mm). The requirement that the facing holes must be aligned with one another along the electron beam restricts the ability to tilt freely the gas-tight cell inside the TEM. This limitation reduced the probability of observing contiguous (00*l*) lattice planes of spheroidal halloysite parallel to the electron beam and thus to record properly oriented electron diffraction patterns. Frequent sudden leaks through the carbon film were the main drawback of the technique. This halted the experiment immediately, reducing the likelihood of making successful observations. This system was, however, preferred to an environmental transmission electron microscope with a differential pumping aperture because it offers: (1) better resolution; (2) the option to introduce different types of gas; and (3) the ability to switch from environmental to vacuum mode easily.

Most of the experiments were performed under a gas pressure of 30 Torr. This pressure corresponds to the sum of the partial pressures of all the gases in the humid air obtained by bubbling clean air into a water tank at 20ºC. Considering that the water-vapor pressure at 100% RH and 1 atmosphere (1 atm = 760 Torr) is equal to 17.55 Torr, a water-vapor pressure of 0.7 Torr can be assumed in the environmental cell (100% RH, 30 Torr). The environmental cell used in this study also allowed reduction of the gas pressure and switching to vacuum mode. Evacuation was achieved inside the cell during the experiment and dynamic observations were made during the process. The microstructure of completely dehydrated spheroidal halloysite was also studied using HRTEM by means of a conventional sample holder under vacuum (JEOL Ltd™, Tokyo, Japan). In this last experiment, particles of halloysite were crushed gently and dispersed on the carbon film of a square mesh copper grid.

RESULTS

Description of spheroidal halloysite in its hydrated state

Particles of halloysite were observed successfully using the EC-TEM with a circulation of air saturated with water vapor at a total gas pressure of 30 Torr. The individual particles displayed an almost regular spheroidal morphology with a mean external diameter of 400 nm (Figure 2). Their outlines appeared polyhedral, which indicated faceting of the external surface. The absorption contrast increased systematically inward, indicating that the particles were filled with matter. The d_{001} was measured using selected area electron diffraction (SAED) at the periphery of the spheroid, *i.e.* where the layer stacking was most visible (Figure 3). The results varied between 10 and 11 Å which was consistent with d_{001} values of fully hydrated halloysite reported in the literature (10.1 Å in Joussein *et al.*, 2005). The observed particles of halloysite were thus considered to be in the hydrated form (*i.e.* 10 Å halloysite).

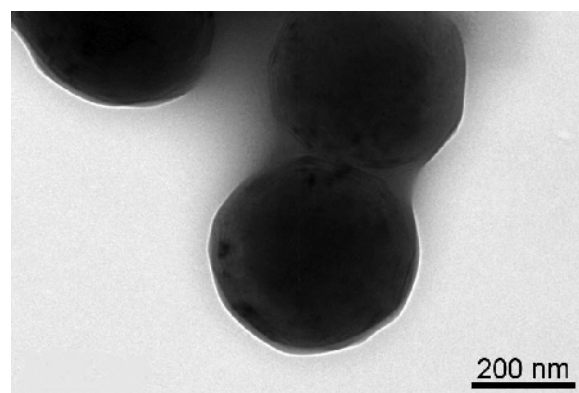

Figure 2. Bright-field view of hydrated spheroidal halloysites observed under environmental conditions in EC-TEM. The dark-gray 'glue' is due to contamination. Note the varying polygonal diffraction contrasts at the peripheries of the polyhedral spheroids.

https://doi.org/10.1346/CCMN.2015.0630503 Published online by Cambridge University Press

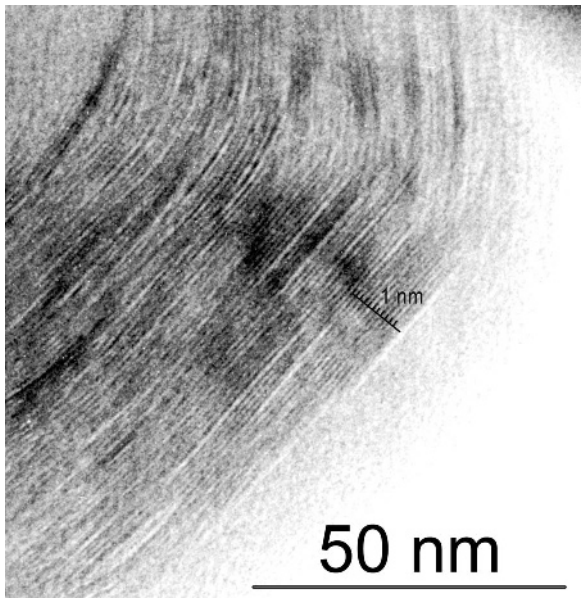

Figure 3. HRTEM image of a spheroidal halloysite on which basal spacing of lattice fringes can be measured (black lines). Note the curvature of the basal lattice planes when crossing sector boundaries (upper left-hand side). Lattice fringes overlap at sector boundaries due to some misalignment.

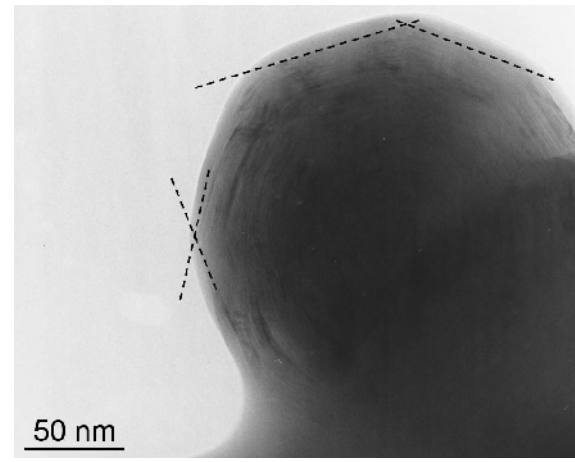

Figure 4. Outline of polyhedral spheroidal halloysite suitably oriented for the measurement of θ angles between facets. Inner layer contrasts are more suitable for measurements than facet outlines as they have not been subjected to contaminant deposition.

The (001) lattice fringes of the different basal layers were observed all around the spheroid, between the faceted surface and the interior (Figure 4). This was representative of their smooth polyhedral morphology. The basal planes ran systematically parallel to the external surface. Planar arrays of layers formed radial sectors of 'planar' halloysite beneath each facet. Neighboring sectors were connected more or less contiguously to the planar lattices by curved layers. The structural layers appeared, on this evidence, to be continuous when passing from one sector to the next. They became increasingly curved from the particle surface inward. Layers were stacked concentrically, which gave an onion-like structure to the particles as a whole.

The angles between neighboring facets were measured in order to further characterize the polyhedral morphology. Considering that the image produced by the TEM is a projection of the object, the observed angle between two neighboring facets is not necessarily the real one. It may be measured reliably only if the (001) planes of contiguous sectors are simultaneously parallel to the electron beam, *i.e.* if their 00*l* reflections are simultaneously present to produce basal lattice fringes in both sectors. The measured angles fluctuated between 18 and 56º and their distribution was fitted by a Gaussian distribution law (Figure 5). The mean value was ~30º, but with significant dispersion. Some angles were measured on particles without visible lattice fringes underneath; sharp facet profiles were added in order to improve statistical representation. Some of these measurements may thus have been acquired on unevenly oriented particles; this provided a reasonable explanation of the noticeable angular dispersion (Figure 5). One group of measurements was distinct from the general trend; note that the mean value of these data (54º) was approximately twice the value of the main mode.

The particles were dehydroxylated progressively and ultimately amorphized after 10 min of exposure to the electron beam. The dehydroxylation due to the electron

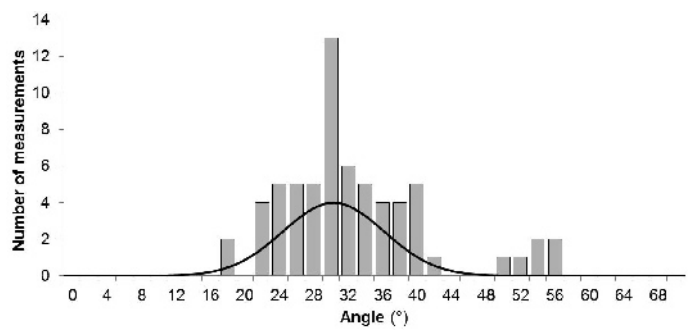

Figure 5. Distribution of the measured inter-facet angles on hydrated halloysites.

https://doi.org/10.1346/CCMN.2015.0630503 Published online by Cambridge University Press

beam was expressed as the formation of small bubbles within the structure which were concentrated along the layers.

Dynamic observations of dehydration

The spheroidal halloysite was subjected to humid-gas withdrawal in order to make dynamic observations of dehydration (Figure 6). The volume surrounding the sample was switched from humid air (Figure 6a) to vacuum, which took several minutes to stabilize (Figure 6b,c,d). After the complete establishment of vacuum, the d_{001} measured had decreased to values ranging from 7 to 8 Å (Figure 6c), which was consistent with fully dehydrated halloysite (7.2 Å in Joussein *et al.*, 2005).

The evolution of the same particles from humid-air flux to vacuum inside the cell was imaged in Figure 6a and b. The time lapse between the two images was ~1 min. The external morphology remained roughly the same except for concave curvature of facets. Areas of low contrast and with crescent-shaped morphology also appeared within the particles (Figure 6b,c,d). These areas corresponded to internal pores (lenticular flaws) delimited by contrasted areas of layer packets ($d_{001} \approx$ 7 Å). The sizes of the internal pores varied from 10 to 200 nm in length and from 2 to 30 nm in width. The layer packets resulting from this splitting process ranged from 9 to 45 nm in thickness (Figure 6c).

Different air pressures were tested to evaluate the level at which halloysite experienced dehydration. When decreasing the pressure from 30 to 20 Torr inside the cell, no area of brighter contrast appeared after 10 min. The pressure was then reduced to 10 Torr and pore formation was observed in some particles 4 min later.

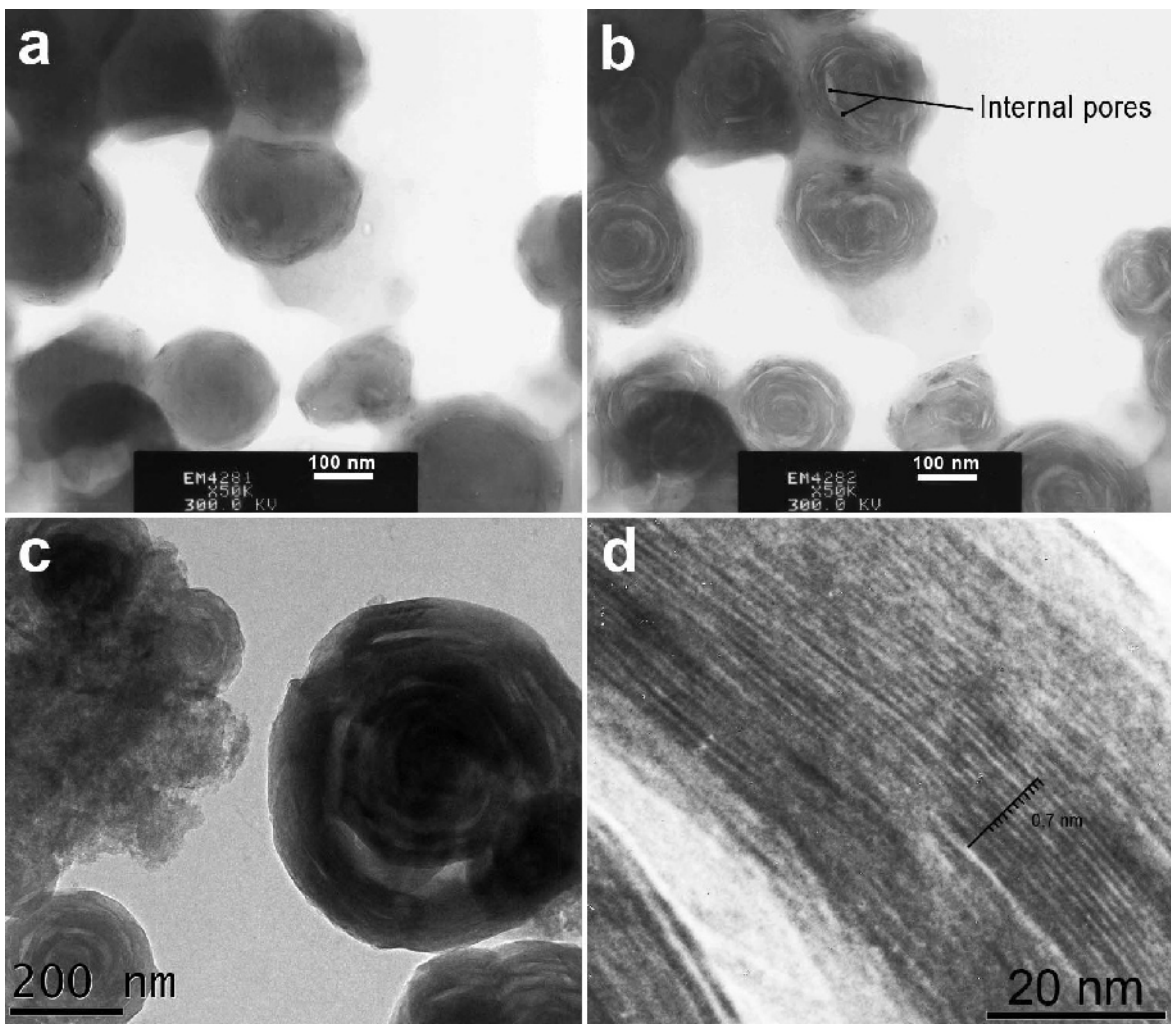

Figure 6. Dynamic observation of the same spheroidal halloysite particles before (a) and after (b) dehydration. [1 min interval between photographs a and b]. (c) Detail of a dehydrated spheroidal particle surrounded by fragments of spheroid caps immersed in allophane (left-hand side). (d) (001) lattice fringes from dehydrated halloysite on which lattice-spacing measurements can be made (black lines).

https://doi.org/10.1346/CCMN.2015.0630503 Published online by Cambridge University Press

When switching to vacuum mode, the primary vacuum (7.5×10^{-5} Torr) was reached within 1 min and then dehydration was complete.

The particle's morphology remained polyhedral after dehydration (Figure 6c). The angles between the facets were measured again on dehydrated particles (Figure 7). Values plotted around 35º and displayed a greater scatter than for hydrated halloysite (Figure 5). During dehydration, the volume of a particle is expected to decrease by at least 30% (*i.e.* d_{001} changes from 10 to 7 Å). For a polyhedron of constant surface, a volume decrease induces a collapse of each facet inward. The facets become concave outward because they are buttressed at their edges by the edges of adjacent facets. This could explain the measured angular increase. Because the observed particle was closed, the collapse was accommodated by: (1) an increase in the angles between the facets; and (2) the formation of internal pores.

Rehydration was also attempted in these experiments. The general aspect of the spheroidal particles remained the same and no evolution of the d_{001} was observed even after several hours of humid-air flux, consistent with a previous study which established that the dehydration of halloysite is irreversible (Alexander *et al.*, 1943).

Microstructure of spheroidal halloysite

The external morphology of the spheroidal halloysite was also studied by scanning electron microscopy (SEM). A JSM 6320 F instrument (JEOL Ltd℠, Tokyo, Japan) with a field emission gun consisting of a cold tungsten cathode was used for this purpose. The sample was deposited on a carbon tape on a pure carbon mount (Structure Probe Incorporation, West Chester, Pennsylvania, USA). A conductive layer of carbon was applied to the sample surface. Observations were made in secondary electron mode using an accelerating voltage of 3 kV and a spot size of 2. The particles of spheroidal halloysite considered were, however, too small to display orientation contrast of facets on spheroids. The particles studied were thus crushed, dispersed on a carbon film, and observed under the TEM with a conventional sample holder. The particles were consequently dehydrated but no significant crystallographic change of the external surfaces was expected, in accordance with the previous observations.

The correlation between facet morphology and crystallography was checked on a fragment of facet belonging to a spheroidal halloysite (referred to hereafter as 'spheroidal cap', see Figure 8). The basic plate was sub-hexagonal in shape (Figure 8a,b). A SAED pattern recorded from this unit allowed indexing of lateral faces as (0 1 −), (0 $\bar{1}$ −), (1 1 −), ($\bar{1}$ $\bar{1}$ −), (1 $\bar{1}$ −), and ($\bar{1}$ 1 −) corresponding to the standard lateral habit of most layered silicates in the C-centered setting (Figure 8c). Based on the relative position of these diffraction spots with respect to the folded edges, the folding axes appeared to run along [0 1 0], [3 1 0], and [3 $\bar{1}$ 0]. These directions corresponded to the three pseudo-equivalent y_i (i = 1, 2, 3) directions of the kaolinite-like structure. They truncated systematically the corners of the sub-hexagonal basic plate. The shape of the spheroid facet was also expected to be sub-hexagonal, but rotated by 30º with respect to it. The curvature of the structure thus occurred along the same axes. To obtain a rough estimate of the number of facets on a supposedly complete spheroid, the surface areas of the spheroids were divided by the surface area of one of the facets. To do so, the width of the facet observed in conventional TEM must correspond to the size of the linear outlines of the polyhedral spheroid measured in EC-TEM. By doing so, the approximate number of 59 ± 20 facets per spheroid was obtained.

DISCUSSION

A complete characterization of spheroidal halloysite in its native hydrated state was performed using EC-TEM. The results allowed us to confirm the native morphology of this mineral and to assess the impact of dehydration on its pore structure. Specifically, the internal pores were shown to have formed progressively through splitting packets of layers during the dehydration process resulting from progressive vacuum (Figure 6). The formation of these pores resulted from the volume decrease of the solid produced artificially and so they should not be referred to as native pores; in

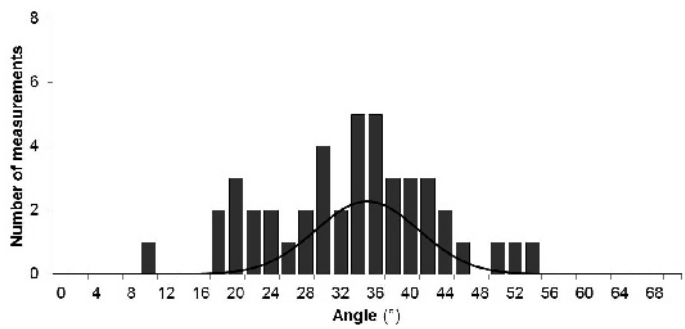

Figure 7. Distribution of the measured inter-facet angles on dehydrated halloysites.

https://doi.org/10.1346/CCMN.2015.0630503 Published online by Cambridge University Press

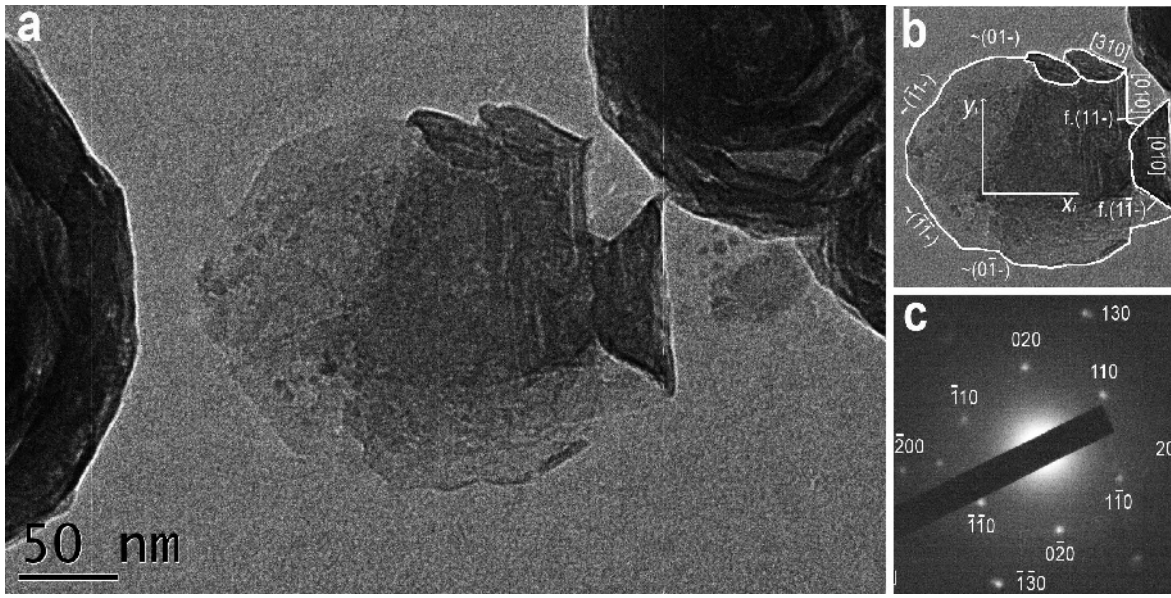

Figure 8. TEM image of a flat pseudo-hexagonal plate of dehydrated halloysite having undergone bending at some corners: (a) rough bright-field image; (b) indexing of outlines as (h k –) where – means undefined l Miller's index; f.(h k –) for 'folded' outline indexing. Directions of folding as [u v w]; all indexing in the standard C-centered a–b unit cell of layer silicates. (c) Selected area electron diffraction (SAED) pattern from the object being used to index part b.

other words, the new pores constituted artificial separations between packets of layers contracted by dehydration. These pores were reported by Kohyama *et al.* (1982) and Churchman *et al.* (1995) to occur only in 7 Å halloysite. The present study has allowed us to document their dynamic formation. The layer contraction caused by dehydration was previously used to explain the polyhedral morphology of halloysite (Tomura *et al.*, 1985). Here, experimental evidence shows that spheroidal halloysite was polyhedral in both its pristine hydrated state, and after dehydration (Figure 6). The process leading to the contraction of the layer drove the formation of internal pores but had little effect on the external morphology of the spheroidal halloysite. The only effect observed was a slight increase in the angle between the facets (Figures 5, 7). This challenges the previous interpretations that the internal pores could be responsible for the physical-chemical properties of halloysite (Askenasy *et al.*, 1973). The absence of internal porosity in the native hydrated state reduces the potential use of spheroidal halloysite as a nano-adsorbent. Tubular halloysite, on the other hand, would be better suited for this purpose because of its unique one-dimensional tubular porous structure (Theng, 1974). Tubular halloysites, whether used as drug carriers or as metal-ion adsorbents, are often studied in the dehydrated state (Tan *et al.*, 2014; Kiani, 2014). As a result, multiple internal pores are observed in the particles along the long tubular pores. In these cases, it is reasonable to assume that this additional porosity was also created during dehydration. Here, the formation of internal pores was shown to be irreversible, raising the question of the connectivity of such pores to the external environment, potentially affecting their contribution to the overall adsorption capacity.

The crystallographic control on the external morphology of halloysite (dioctahedral 1:1 layer silicate) can be discussed with respect to the observations made and a structural analogy with the serpentine family (trioctahedral 1:1 layer silicate). Here, a fragment of a spheroidal cap of sub-hexagonal shape displayed lateral faces indexed (0 1 –), (0 $\bar{1}$ –), (1 1 –), ($\bar{1}$ $\bar{1}$ –), (1 $\bar{1}$ –), and ($\bar{1}$ 1 –) (see Figure 8). The folding axes constituting the spheroids thus appeared to run along [0 1 0], [3 1 0], and [3 $\bar{1}$ 0] corresponding to the three pseudo-equivalent y_i (i = 1, 2, 3) directions of the kaolinite-like structure. Serpentines display the same set of morphologies: tabular, tubular, and polyhedral spheroidal (Zega *et al.*, 2006; Baronnet *et al.*, 2007; Andreani *et al.*, 2008). Compared to spheroidal halloysite, the polyhedral serpentine shows almost equilateral triangular facets, the edges and the inter-facet angles of which are controlled by the crystallographic structure (Baronnet *et al.*, 2007). Regarding their morphologies, therefore, the layer wrapping of these 1:1 phyllosilicates seems to occur as follows: layers of chrysotile (most common tubular serpentine) wrap around one of the pseudo-equivalent crystallographic x_i (i = 1, 2, or 3) axes whereas layers of tubular halloysite do so around one of the pseudo-equivalent crystallographic y_i (i = 1, 2, or 3) axes; layers of polyhedral serpentine (spheroidal serpentine) curve around all three crystallographic y_i (i = 1, 2, 3) axes as do layers of spheroidal halloysite; triangular facets of polyhedral serpentine use a

https://doi.org/10.1346/CCMN.2015.0630503 Published online by Cambridge University Press

once-each pseudo-equivalent y_i direction to bind a facet whereas spheroidal halloysite does so using a twice-each pseudo-equivalent y_i direction to bind hexagonal facets.

In order to maintain lateral continuity of the layer structure, the curvature along any axis implies an interlayer glide normal to it. An anti-symmetric glide must therefore be permitted in spheroidal halloysite whereas it is forbidden in polyhedral serpentine (Baronnet *et al.*, 2007). This difference was presumably due to less restrictive glide directions in halloysite, because of the organization of interlayer water molecules. The water molecules in 10 Å kaolinite were suggested by Tarasevich and Gribina (1972) and Costanzo and Giese (1985) to be bonded with: (1) each other ("associated water"); (2) the oxygen of the tetrahedral sheet ("hole water"); and (3) the hydroxyls of the octahedral sheet. This suggestion is not realistically transposable to halloysites because of the various behaviors displayed during dehydration, implying that water molecules must have different types of bonding within halloysites, ultimately depending on crystal chemistry and morphology (Joussein *et al*., 2006).

Spheroidal halloysites are known to occur as weathering products of volcanic ash. A dissolution-crystallization sequence: volcanic ash−allophane−10 Å halloysite −7 Å halloysite−kaolinite is widely accepted (*e.g.* Tomura *et al.*, 1985; Churchman, 2000). This sequence is consistent with the observations made on the sample from Opotiki studied here. The bulk sample of halloysite spheroids (examined at any stage of their development) displayed particles surrounded by polyhedral caps resembling turtle shells and immersed in an allophane assemblage of nano spherules (Figure 6c). This would suggest that spheroidal halloysites grew at the expense of an allophane precursor. Nucleation of spheroids may start from peripheral layers as caps. This nucleation would evolve to a more or less complete spheroid by lateral growth, further faceting, and infilling of the concave side by new layers including formation of the spheroid core (*i.e.* centripetal growth). On the one hand, the addition of a small quantity of aluminum during tubular chrysotile synthesis suppresses growth in length, thereby leading to an increase in diameter (Grauby and Baronnet, 2009). Those authors also observed curved layers capping the end of tubes as in sugar tongs. The layers curve around the *y* axis implying a sudden change in the bending axis. On the other hand, polyhedral serpentines are never observed in purely magnesium synthesis experiments; instead their formation is possible only when the system is enriched with Al or Fe (III). Grauby and Baronnet (2009) also observed short tubes acting as nuclei in the centers of the polyhedral serpentines. Those authors proposed that when a tube of chrysotile contacts a solution enriched in trivalent cations, its growth in length is blocked and the direction of layer wrapping changes. This process is attributed to an early stage of formation of polyhedral serpentines (1:1 trioctahedral) which seems to be allowed only in a growth medium enriched in trivalent cations. In the case of 1:1 dioctahedral phyllosilicates, Petit *et al.* (1995) showed that spheroidal kaolinite synthesis was possible in Cu^{2+}-, Ni^{2+}-, or Zn^{2+}-enriched systems. The central role played by the octahedral site occupancy in the formation of the different microstructures of 1:1 phyllosilicates can thus be expected. The spheroidal morphology seems favored by the presence of trivalent cations in octahedral sites for the 1:1 trioctahedral phyllosilicates whereas it seems favored by the presence of divalent cations for 1:1 dioctahedral phyllosilicates. The formula unit of the spheroidal halloysite ($Al_{1.86}Fe_{0.14}(OH)_4Si_{1.98}Al_{0.02}O_5$) studied by Churchman and Theng (1984) assumes that all Fe is in the ferric state Fe (III). Octahedral iron could, however, be partly in the ferrous state Fe (II). Further characterization by Mössbauer spectroscopy is needed in order to solve this issue. If confirmed, a pre-existent tubular halloysite particle would experience a cessation of growth as a response to the incorporation of divalent cations from a solution rich in divalent cations. The incorporation and/or adsorption of these cations inside and/or on the structure (*i.e.* octahedral substitution) would lead to no change in the *y*-wrapping axis but to the use of all three pseudo equivalent y_i axes instead of only one. Further growth will thus produce spheroidal halloysites overgrowing tubular halloysites. Nevertheless, no short tubes have yet been observed within the particles of spheroidal halloysites. This could be due to the fact that TEM images are a projection of the objects. The thicknesses at the centers of spheroidal particles and microstructure superimposition features may thus impede the recording of clear images at these locations. Only observations of ultra-microtome sections made through the spheroidal halloysite particles under HRTEM might provide evidence of a possible coexistence between tubular and spheroidal halloysite.

CONCLUSIONS

Natural mineral materials are used increasingly as nano-adsorbents. Halloysites are considered to be good candidates to load and release metal ions or organic molecules because of their specific porous structure. The porosity and water content of these 1:1 phyllosilicates are, however, influenced significantly by their hydration state. Here, the native morphology and internal porous structure of spheroidal halloysite from Opotiki (New Zealand) in its native hydrated state were characterized using EC-TEM. The isolated particles in their pristine state displayed a polyhedral external surface with layers stacked concentrically. Dynamic observations during dehydration showed that the external morphology remained unaffected, but internal pores formed through this process. They corresponded to the separation between layer packets contracted by the loss of water

https://doi.org/10.1346/CCMN.2015.0630503 Published online by Cambridge University Press

molecules (d_{001} decreased from 10 to 7 Å). A rehydration experiment showed that the formation of these pores was irreversible, *i.e.* water molecules could not be reintegrated into the crystal structure. The connectivity of such pores to the external environment and hence their accessibility to metal ions or organic molecules must, therefore, be further addressed. Similar internal pores are present within the walls of dehydrated tubular halloysite. In both cases, their contribution to the overall adsorption properties would have to be clarified.

Using HRTEM, isolated facets were also observed and they displayed a pseudo-hexagonal morphology. The three-dimensional microstructure of the spheroid appeared bent along the three pseudo-equivalent y_i directions of the kaolinite-like single layers. An analogy with polyhedral serpentine has allowed us to propose a formation process for hydrated spheroidal halloysite. This process would start with tubular halloysite particles, growth of which is suppressed by the entry of divalent cations into the growth medium. No change of the wrapping around y axis will be induced but all three y_i axes will now be involved. Ultimately, spheroidal halloysite would be produced by the successive wrapping of numerous layers. This change in the wrapping mode implies an anti-symmetric glide normal to the former axis owing to the organization of the water molecules within the structure. If this formation mechanism is confirmed, it would result in the coexistence of tubular and spheroidal halloysite within natural deposits. The complete understanding of the growth mechanism of hydrated halloysite would ultimately benefit from further characterization of the organization of interlayer water molecules.

ACKNOWLEDGMENTS

The authors thank Serge Nitsche (CINaM-CNRS) for his helpful and careful advice on electron microscopy. The CNRS-INSU is acknowledged for having partly funded the environmental cell used in this study as a 'National Instrument for Earth Science' research project. The work was carried out within the framework of the ICoME2 Labex (ANR-11-LABX-0053) and the A*MIDEX projects (ANR-11-IDEX-0001-02) co-funded by the French program 'Investissements d'Avenir' which is managed by the ANR, the French National Research Agency. The authors are grateful to the Editor-in-Chief (Michael A. Velbel) as well as to the two anonymous reviewers who helped to improve the manuscript by means of constructive reviews.

REFERENCES

Alexander, L.T., Faust, G.T., Hendricks, S.B., Insley, H., and McMurdie, H.F. (1943) Relationship of the clay minerals halloysite and endellite. *American Mineralogist*, **28**, 1–18.

Andreani, M., Grauby, O., Baronnet, A., and Munoz, M. (2008) Occurrence, composition and growth of polyhedral serpentine. *European Journal of Mineralogy*, **20**, 159–171.

Askenasy, P.E., Dixon, J.B., and McKee, T.R. (1973) Spheroidal halloysite in a Guatemalan soil. *Soil Science Society of America Journal*, **37**, 799–803.

Bailey, S.W. (1990) Halloysite – A critical assessment. Pp. 89–98 in: *Surface Chemistry Structure and Mixed Layering of Clays*, *Proceedings of the 9th International Clay Conference*, *Strasbourg, 1989, Volume II* (V.C. Farmer and Y. Tardy, editors). Sciences Géologiques Memoire **86**.

Baronnet, A., Andreani, M., Grauby, O., Devouard, B., Nitsche, S., and Chaudanson, D. (2007) Onion morphology and microstructure of polyhedral serpentine. *American Mineralogist*, **92**, 687–690.

Bates, T.F., Hildebrand, F.A., and Swineford, A. (1950) Morphology and structure of endellite and halloysite. *American Mineralogist*, **6**, 237–248.

Chisholm, J.E. (1992) The number of sectors in polygonal serpentine. *The Canadian Mineralogist*, **30**, 355–365.

Churchman, G.J. and Carr, R.M. (1975) The definition and nomenclature of halloysites. *Clays and Clay Minerals*, **23**, 382–388.

Churchman, G.J. and Theng, B.K.G. (1984) Interactions of halloysites with amides: mineralogical factors affecting complex formation. *Clay Minerals*, **19**, 161–175.

Churchman, G.J., Davy, T.J., Aylmore, L.A.G., Gilkes, R.J., and Self, P.G. (1995) Characteristics of fine pores in some halloysites. *Clay Minerals*, **30**, 89–98.

Churchman, G.J. (2000) The alteration and formation of soil minerals by weathering. Pp. 3–76 in: *Handbook of Soil Science* (M.E. Sumner, editor). CRC Press, Boca Raton, Florida, USA.

Costanzo, P.M. and Giese, R.F. (1985) Dehydration of synthetic hydrated kaolinites: a model for the dehydration of halloysite (10 Å). *Clays and Clay Minerals*, **33**, 415–423.

Delvaux, B., Herbillon, A.J., and Vielvoye, L. (1990) Surface properties and clay mineralogy of hydrated halloysitic soil clays. I. Existence of interlayer K^+ specific sites. *Clay Minerals*, **25**, 129–139.

Giese, R.F. (1991) Kaolin minerals: structures and stabilities. Pp. 29–66 in: *Hydrous Phyllosilicates (Exclusive of Micas)* (S.W. Bailey, editor). Reviews in Mineralogy, **19**. Mineralogical Society of America, Washington, D.C.

Grauby, O. and Baronnet, A. (2009) Synthesis of polyhedral serpentine. *XIV International Clay Conference*, Italy, Abstract vol. 2, p. 466.

Guggenheim, S. (1977) Introduction to the properties of clay minerals. Pp. 371–388 in: *Teaching Mineralogy* (J. Brady, D. Mogk, and D. Perkins, editors). Mineralogical Society of America, Washington, D.C.

Joussein, E., Petit, S., Churchman, J., Theng, B., Righi, D., and Delvaux, B. (2005) Halloysite clay minerals – a review. *Clay Minerals*, **40**, 383–426.

Joussein, E., Petit, S., Fialips, C-I., Vieillard, P., and Righi, D. (2006) Differences in the dehydration-rehydration behavior of halloysites: new evidence and interpretations. *Clays and Clay Minerals*, **54**, 473–484.

Joussein, E., Petit, S., and Delvaux, B. (2007) Behavior of halloysite clay under formamide treatment. *Applied Clay Science*, **35**, 17–24.

Kiani, G. (2014) High removal capacity of silver ions from aqueous solution onto halloysite nanotubes. *Applied Clay Science*, **90**, 159–164.

Kirkman, J.H. (1977) Possible structure of halloysite disks and cylinders observed in some New Zealand tephras. *Clay Minerals*, **12**, 199–215.

Kohyama, N., Fukushima, K., and Fukami, A. (1978) Observation of the hydrated form of tubular halloysite by an electron microscope equipped with an environmental cell. *Clays and Clay Minerals*, **26**, 25–40.

Kohyama, N., Fukushima, K., and Fukami, A. (1982) Interlayer hydrates and complexes of clay minerals observed by electron microscopy using an environmental cell. Pp. 373–384 in: *Proceedings of the 7th International Clay*

Conference (1981) Bologna, Italy (F.V.H. van Olphen, editor). Elsevier, Amsterdam.

MacEwan, D.M.C. (1948) Complexes of clay with organic compounds. I. Complex formation between montmorillonite and halloysite and certain organic liquids. *Journal of the Chemical Society Faraday Transactions*, **44**, 349–367.

Parham, W.E. (1970) Halloysite-rich tropical weathering products of Hong-Kong. Pp. 403–416 in: *Proceeding of the International Clay Conference, Tokyo, Japan*, *1969*.

Petit, S., Decarreau, A., Mosser, C., Ehret, G., and Grauby, O. (1995) Hydrothermal synthesis (250ºC) of copper-substituted kaolinites. *Clays and Clay Minerals*, **43**, 482–494.

Radoslovich, E.W. (1963) The cell dimensions and symmetry of layer-lattice silicate. VI. Serpentine and kaolin morphology. *American Mineralogist*, **48**, 368–378.

Sand, L.B. (1956) On the genesis of residual kaolin. *American Mineralogist*, **41**, 28–40.

Tarasevich, Y.I. and Gribina, I.A. (1972) Infrared spectroscopy study of the state of water in halloysite. *Kolloidnyi Zhurnal*, **34**, 405–411.

Tan, D., Yuan, P., Annabi-Bergaya, F., Liu, D., Wang, L., Liu, H., and He, H. (2014) Loading and *in vitro* release of ibuprofen in tubular halloysite. *Applied Clay Science*, **96**, 50–55.

Theng, B.K.G. (1974) *The Chemistry of Clay-Organic Reactions*. Adam Hilger, London.

Tomura, S., Shibasaki, Y., Mizuta, H., and Kitamura, M. (1985) Growth conditions and genesis of spherical and platy kaolinite. *Clays and Clay Minerals*, **33**, 200–206.

Zega, T.J., Garvie, L.A.J., Dodony, I., Friedrich, H., Stroud, R.M., and Buseck, P.R. (2006) Polyhedral serpentine grains in CM chondrites. *Meteoritics and Planetary Science*, **41**, 681–690.

(*Received 21 October 2014; revised 26 November 2015; Ms. 924; AE: M.A. Velbel*)